THE JOURNAL OF BIOLOGICAL CHEMISTRY VOL. 283, NO. 30, pp. 20864–20873, July 25, 2008

Control of Translocation through the Sec61 Translocon by Nascent Polypeptide Structure within the Ribosome*[S]◆

Received for publication, May 8, 2008 Published, JBC Papers in Press, May 13, 2008, DOI 10.1074/jbc.M803517200

Colin J. Daniel[‡], Brian Conti[‡], Arthur E. Johnson[§], and William R. Skach[‡1]

From the [‡]Department of Biochemistry & Molecular Biology, Oregon Health & Science University, Portland, Oregon 97239 and the [§]Department of Molecular and Cellular Medicine and the Departments of Chemistry and of Biochemistry and Biophysics, Texas A&M University System Health Science Center, College Station, Texas 77843-1114

During polytopic protein biogenesis, multiple transmembrane segments (TMs) must pass through the ribosome exit tunnel and into the Sec61 translocon prior to insertion into the endoplasmic reticulum membrane. To investigate how movement of a newly synthesized TM along this integration pathway might be influenced by synthesis of a second TM, we used photocross-linking probes to detect the proximity of ribosome-bound nascent polypeptides to Sec61α. Probes were inserted at sequential sites within TM2 of the aquaporin-1 water channel by *in vitro* translation of truncated mRNAs. TM2 first contacted Sec61α when the probe was positioned ~38 residues from the ribosome peptidyltransferase center, and TM2-Sec61α photoadducts decreased markedly when the probe was >80 residues from the peptidyltransferase center. Unexpectedly, as nascent chain length was gradually extended, photocross-linking at multiple sites within TM2 abruptly and transiently decreased, indicating that TM2 initially entered, withdrew, and then re-entered Sec61α. This brief reduction in TM2 photocross-linking coincided with TM3 synthesis. Replacement of TM3 with a secretory reporter domain or introduction of proline residues into TM3 changed the TM2 cross-linking profile and this biphasic behavior. These findings demonstrate that the primary and likely secondary structure of the nascent polypeptide within the ribosome exit tunnel can influence the timing with which topogenic determinants contact, enter, and pass through the translocon.

Protein translocation into the endoplasmic reticulum (ER)[2] is initiated when a signal sequence emerges from the ribosome, binds a signal recognition particle, and targets the ribosome-nascent chain complex to the Sec61 translocon (1–3). As the signal sequence engages Sec61α, the nascent polypeptide is directed through an aqueous channel that extends from the exit tunnel of the 60 S ribosome subunit, through the translocon pore and into the ER lumen (4–7). Secretory and transmembrane proteins usually traverse this pathway coincident with protein synthesis and contact translocon components (*e.g.* Sec61α) when the nascent chain has extended >30 residues beyond the ribosome peptidyltransferase center (PTC) (8–11). However, polypeptide elongation does not provide the sole driving force for ribosome-dependent translocation because, under certain circumstances, vectoral transport can be uncoupled from protein synthesis. Unfolded, ribosome-attached protein domains can be efficiently transported into the ER lumen after synthesis (12–15), and ribosome-attached polypeptides can move from the ER lumen back into the cytosol (16, 17). Net anterograde movement is therefore controlled by several factors, including polypeptide folding, attachment of *N*-linked glycans, interaction with ER chaperones, and ultimately, release of the nascent polypeptide following peptidyl-tRNA bond cleavage (16, 18–20).

In contrast to events in the ER lumen, relatively little is known regarding how vectoral movement of the nascent polypeptide is controlled within the ribosome exit tunnel. This is particularly important for the co-translational integration of polytopic membrane proteins because the timing with which topogenic determinants interact with the translocon and/or ribosome is critical for establishing transmembrane topology. Experiments monitoring accessibility of a secretory protein reveal that shortly after ribosome-nascent chain complex targeting, the nascent chain in the ribosome exit tunnel becomes inaccessible to both cytosolic and ER lumenal compartments (5, 21). As translation resumes, the signal sequence engages Sec61α (22, 23), and an aqueous pore is opened through the translocon that provides the nascent chain access to the ER lumen (5). Shortly after the synthesis of a transmembrane segment (TM), the lumenal end of the translocon pore is closed by the action of BiP, and the cytosolic end is opened, thereby redirecting the growing polypeptide to the cytosol (21, 24–26). These latter events occur coincident with folding of the TM into an α-helical or near helical conformation inside the ribosome exit tunnel at a site close to the PTC (27). Nascent chain folding inside the ribosome therefore appears to be an important regulatory mechanism for the topogenesis and hence integration of single-spanning membrane proteins. What then happens during the synthesis of proteins that contain multiple

* This work was supported, in whole or in part, by National Institutes of Health Grants DK51818 and GM53457 (to W. R. S.) and GM26494 (to A. E. J.). This work was also supported by American Heart Association Established Investigator Grant and Grant-in-aid 0755832Z (to W. R. S.) and Robert A. Welch Foundation Chair Grant BE-0017 (to A. E. J.).The costs of publication of this article were defrayed in part by the payment of page charges. This article must therefore be hereby marked "*advertisement*" in accordance with 18 U.S.C. Section 1734 solely to indicate this fact.

◆ This article was selected as a Paper of the Week.

[S] The on-line version of this article (available at http://www.jbc.org) contains supplemental Fig. 1.

[1] To whom correspondence should be addressed: Dept. of Biochemistry & Molecular Biology, Oregon Health & Science University, L-224, 3181 S. W. Sam Jackson Park Rd., Portland, OR 97239. Fax: 503-494-8393; E-mail: skachw@ohsu.edu.

[2] The abbreviations used are: ER, endoplasmic reticulum; PTC, peptidyltransferase center; TM, transmembrane segment; AQP1, aquaporin-1; aa, amino acid(s); ϵANB, N^{ϵ}-(5-azido-2-nitrobenzoyl).

TMs? Does each TM fold into a compact structure within the ribosome? When connecting loops between TMs are short, does the presence of multiple TMs at different locations along this pathway influence the vectoral process of translocation? If such folding occurs, how does its timing and location influence the presentation of sequential topogenic determinants to the translocon?

To address these questions, we examined the molecular environment of an internal TM (TM2) in the aquaporin-1 (AQP1) water channel as it exited the ribosome and entered the Sec61 translocon. Aquaporins compose a widely expressed family of homotetrameric polytopic proteins that selectively transport water and/or glycerol across cell membranes (28). They exhibit a highly conserved topology in which six TMs, four short connecting loops, and two half-TMs are arranged in an hourglass configuration around a monomeric pore (29, 30). In the case of AQP1, TM2 is somewhat atypical in that it transiently passes through the translocon before acquiring its membrane-spanning topology because two polar residues at its N terminus prevent it from efficiently terminating translocation (31–34). As with other aquaporins, TM2 is flanked on its N and C termini by relatively short peptide loops (13 and 23 amino acids (aa), respectively) (30) such that TM1, TM2, and TM3 simultaneously reside within or closely adjacent to the ribosome-translocon complex (11).

In this study, a single photocross-linking probe was incorporated individually at six successive sites within AQP1 TM2, and its efficiency of cross-linking to Sec61α was monitored at sequential stages of synthesis using arrested integration intermediates. As expected, TM2 cross-linking was highly dependent upon the length of the nascent polypeptide between the probe and the PTC. Surprisingly, as nascent chain length was gradually extended, a complex pattern of photoadduct formation was observed in which TM2 initially entered, withdrew, and then re-entered Sec61α during a very brief period that corresponded to TM3 synthesis. Replacement of TM3 with a secretory reporter domain or introduction of proline residues into TM3 eliminated this biphasic cross-linking behavior. These results demonstrate that nascent chain movement through the translocon can be directly influenced by the structure of the nascent polypeptide within the ribosome exit tunnel.

EXPERIMENTAL PROCEDURES

Plasmid Construction—Plasmid pSP64-CHIP28 (31) was used to create ΔK mutants by replacing lysine with arginine codons at residues 6–8, 36, 51, and 243 in human AQP1 cDNA using PCR overlap extension (35). Complementary primers for AQP1 encoding the desired arginine codon(s) were used in parallel PCRs, along with upstream and downstream primers. Vent DNA polymerase (New England Biolabs, Beverly, MA) was used for all PCRs according to the manufacturer's directions. The PCR fragments were amplified in a second round of PCR to generate AQP1 fragments containing the engineered codon. Silent mutations were introduced in some constructs for screening purposes. PCR fragments were digested either with NcoI and AvaI or with AvaI and BamHI (3′-polylinker) depending on the location of the arginine codon and religated into a similarly digested pSP64-CHIP28 plasmid. Single lysine codons were then engineered into the AQP1ΔK templates at residues 56–61, and mutations C102P and V103P were made using the same approach. AQP1 fusion proteins (described previously (31)) were modified by converting endogenous lysine residues in the prolactin-derived reporter to arginine and inserting lysine codons at AQP1 residues 56–58. The correct sequences of all PCR-amplified DNAs were verified by sequencing.

In Vitro Transcription and Translation—AQP1 cDNA was amplified by PCR using *Taq* DNA polymerase (New England Biolabs) with a 5′-oligonucleotide complementary to pSP64 bp 2757 (AGGATCTGGCTAGCGATCACC) and a 3′-oligonucleotide complementary to the AQP1 coding sequence. Most 3′-oligonucleotides contained an additional codon beyond the last amplified AQP1 codon such that truncated nascent chains ended with Gly to equalize spontaneous peptidyl-tRNA hydrolysis of translocation intermediates (data not shown). The final lengths of amplified AQP1 polypeptides (including the glycine) were 94, 97,102, 105, 107,110, 115, 118, 123, 126, 140, 143, 154, 158, 173, 217, and 267 residues as indicated. PCR products were transcribed *in vitro* using SP6 polymerase (Epicenter, Madison, WI) at 40 °C for 1 h in 20-μl reactions as described (36). Transcripts were extracted with phenol/chloroform and stored at −80 °C.

Translations were carried out for 1 h at 25 °C in reactions containing 40% (v/v) hemin-supplemented rabbit reticulocyte lysate, canine pancreas microsomal membranes ($A_{280} = 4–6$), and 1 μCi/μl Tran^{35}S-label as described previously (36) with the following modifications. Reactions were supplemented with each of 18 essential amino acids (not Met or Lys) at 40 μM, and dithiothreitol was replaced with 2 mM reduced glutathione. Where indicated, N^{ϵ}-(5-azido-2-nitrobenzoyl-[^{14}C]Lys-tRNA^{Lys} (ϵANB-Lys-tRNA) was added to a final concentration of 0.8–1.0 pmol/μl to achieve an incorporation efficiency of ~50%, and puromycin (1 mM final concentration) was incubated with ribosome-nascent chain complexes for 10 min at 24 °C. All reactions containing the ϵANB probe were assembled and carried out in a darkroom under safelight conditions.

Photocross-linking Nascent Chain Intermediates—ϵANB-Lys-tRNA was prepared from unfractionated yeast tRNA (Roche Applied Science) that had been purified by two cycles of fast protein liquid chromatography (Mono Q 10/10 column, Amersham Biosciences) to yield tRNA^{Lys}, aminoacylated with [^{14}C]Lys using *Escherichia coli* aminoacyl-tRNA synthetases, and reacted with the *N*-hydroxysuccinimide ester of ϵANB (Pierce) as described previously (37). Microsomal membranes containing radiolabeled nascent chain intermediates were collected by pelleting for 10 min at 180,000 × *g* through 0.5 M sucrose in Buffer A (50 mM HEPES-KOH (pH 7.5), 0.1 M KOAc (pH 7.5), 5 mM $Mg(OAc)_2$, and 1 mM reduced glutathione). Membrane pellets were resuspended in 0.1 M sucrose in Buffer A. In all experiments, microsomal membranes were added to translation reactions to achieve a targeting efficiency of >90% based on translocation of a secretory control protein (supplemental Fig. 1). AQP targeting efficiency was confirmed by flotation experiments in which truncated integration intermediates were quantitatively recovered (~90%) in floated microsomal membrane fractions (supplemental Fig. 1). Thus, nascent chains collected by pelleting were properly targeted to

the membrane and did not represent misfolded aggregates. Samples were photolyzed by UV irradiation for 10 min on ice as described previously (11). Samples were rotated every 2 min during UV exposure and then stored at −80 °C.

Acid Precipitation and Normalization of Translation Products—To normalize for variation in yield during translation and membrane resuspension, duplicate aliquots from resuspended microsome samples were incubated (37 °C, 10 min) in 1 M NaOH and 2% (v/v) H_2O_2 to bleach the heme and then precipitated in 10% (w/v) trichloroacetic acid and 3% (w/v) casamino acids at 85 °C for 10 min. Precipitates were collected on 45-μm Durapore filters (Millipore, Billerica, MA), washed twice with 5% (w/v) trichloroacetic acid, and air-dried. Total precipitated ^{35}S-labeled protein was quantified by scintillation counting. Net mRNA-dependent cpm was obtained by the difference in hot acid-precipitable cpm of identically treated translation samples lacking mRNA transcript. Alternatively, some translation products were quantitated by phosphorimaging of non-UV light-irradiated samples as described previously (11).

Immunoprecipitation and Photocross-linking Efficiency—Equivalent amounts of radioactive translation products were diluted in 100 μl of 1% (w/v) SDS and 0.1 M Tris-HCl (pH 8) and denatured at 37 °C for 30 min. Samples were then diluted in 1 ml of Buffer B (1% (v/v) Triton X-100, 0.1 M NaCl, 0.1 M Tris-HCl (pH 8), and 10 mM EDTA (pH 8)) and mixed on ice with 1 μl of peptide-specific Sec61α antisera (raised against peptide AIKFLEVIKPGCC, generously provided by Dr. Kent Matlack) and 5 μl of protein A-Affi-Gel (Bio-Rad). Samples were rotated overnight at 4 °C and washed three times with 0.5 ml of ice-cold Buffer B and twice with 0.5 ml of 0.1 M NaCl and 0.1 M Tris-HCl (pH 8) prior to separation on 12–17% (w/v) SDS-polyacrylamide gels. Immunoprecipitations were performed simultaneously for all probe sites and truncations in a given experiment, and gels were exposed together on a single phosphorimaging screen (Eastman Kodak Co.). Bands were quantitated using a Bio-Rad FX molecular imager with Quantity One software. Background signal (ΔK control) was subtracted from each corresponding Lys-containing band to obtain the net Sec61α-photoadduct signal. Net signals for each truncation and probe incorporation site were then divided by the total signal obtained for the entire experiment to determine the relative cross-linking efficiency at a given site and truncation. This enabled us to average results from repeat experiments and to account for differences in translation, pellet recovery, immunoprecipitation efficiency, screen exposure times, and ^{35}S decay. Thus, each value plotted in Figs. 4–6 represents the cross-linking efficiency at a given probe site relative to the cross-linking at all probe sites and at all truncations examined in the entire experiment. Photocross-linking efficiency at each site was then plotted as a function of nascent chain length. All plotted data are an average of at least two independent experiments. Statistical analysis was performed using Student's *t* test (see Fig. 5*C*), and *error bars* represent S.E.

RESULTS

Experimental Strategy—To monitor nascent chain movement through the ER translocon, we developed a semiquantitative technique to determine the relative proximity of the nascent polypeptide to the major translocon component, Sec61α (11). Integration intermediates containing AQP1 polypeptides of defined length were generated by translating truncated mRNAs, *i.e.* lacking a terminal stop codon, in rabbit reticulocyte lysate supplemented with canine pancreatic ER microsomal membranes. A photoactive cross-linking probe was incorporated at a unique engineered Lys residue in AQP1 by including a modified tRNA, ϵANB-Lys-tRNA, in the translation reaction (37). Because removal of the stop codon allows the nascent polypeptide to remain tethered to the ribosome via its covalent peptidyl-tRNA bond, the position of the probe along the translocation pathway can be controlled by the site of mRNA truncation and the location of the Lys codon in the mRNA. Upon UV irradiation, the ϵANB moiety is converted to a highly reactive and short-lived nitrene group that can form a single covalent cross-link by insertion into ubiquitous C-H and N-H sites or by reaction with nucleophiles (*e.g.* primary amines) via ring expansion. The prominent availability of these sites allows the nitrene to cross-link virtually any adjacent protein within reach of the 12-Å spacer arm (37). Because of this promiscuous, albeit variable, reactivity to a variety of chemical groups, the relative efficiency of photoadduct formation provides a means to compare the relative proximity of the nitrene probe to neighboring translocon components (9, 11, 37–40).

AQP1 Integration Intermediates Cross-link Sec61α—Wild-type AQP1 truncated at codon 134 contains five endogenous lysine residues at positions 6, 7, 8, 36, and 51. When translated *in vitro*, roughly half of the nascent chains undergo *N*-linked glycosylation at Asn^{42} within the TM1-TM2 connecting loop (31) to generate two ^{35}S-labeled AQP1 peptides that migrated at apparent sizes of ~14 and 17 kDa (Fig. 1*A*). This level of glycosylation is similar to that observed *in vivo* and is likely limited by the short loop connecting TM1 and TM2, which restricts access of Asn^{42} to oligosaccharyltransferase. Following UV irradiation, protein translated in the presence of ϵANB-Lys-tRNA underwent an ~38-kDa shift in migration (Fig. 1*A*, *lane 6*). This photoadduct was not observed in the absence of either UV exposure (*lane 5*) or ϵANB-Lys-tRNA (*lanes 1–4*) or if nascent chains were first released from the PTC by puromycin-mediated cleavage of the peptidyl-tRNA bond (*lanes 7* and *8*). Formation of the photoadduct therefore required both ϵANB probe incorporation and an intact physiological integration intermediate. Immunoprecipitation of translation products with peptide-specific antisera identified the major cross-linked protein as Sec61α (Fig. 1*B*, *lane 2*). Cross-links to TRAM were also identified but, in all cases, were severalfold less robust than those observed for Sec61α and could not be accurately quantified (data not shown). Subsequent experiments therefore focused on AQP1-Sec61α interactions.

Site-specific Photocross-linking of TM2 to Sec61α—Photoreactive probes were next incorporated at specific residues by converting endogenous lysine codons to arginine to generate a lysine-less (ΔK) AQP1 template. Individual Lys codons were then engineered into AQP1ΔK near the center of TM2 at adjacent residues Ser^{59}, Ile^{60}, and Ala^{61} to investigate the cross-linking efficiencies along different faces of the TM2 helix. We focused on TM2 because AQP1 is efficiently targeted to the ER

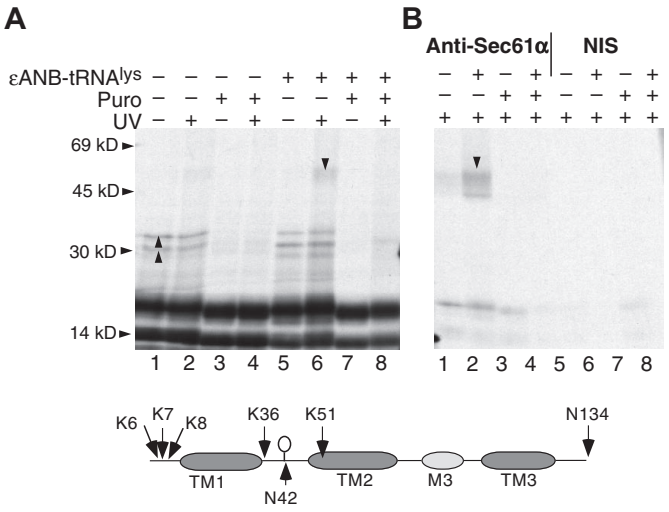

FIGURE 1. **ϵANB-dependent cross-linking to Sec61α.** *A*, AQP1 cDNA was truncated at codon 134, translated in reticulocyte lysate in the presence or absence of ϵANB-Lys-tRNA, and analyzed by SDS-PAGE and autoradiography. Samples were treated with puromycin (*Puro*) and UV irradiation as indicated. Major bands with apparent sizes of 14 and 17 kDa represent non-glycosylated and glycosylated polypeptides, respectively. The *downward arrowhead* (*lane 6*) shows the ~55-kDa photoadduct. The *upward arrowheads* (*lane 1*) indicate residual peptidyl-tRNA bands that survived SDS-PAGE. These bands were independent of UV light and eliminated by both puromycin (*lanes 3* and *4*) and RNase digestion (data not shown). *B*, irradiated samples were denatured and immunoprecipitated with Sec61α antisera (*lanes 1–4*) or nonimmune sera (*NIS*; *lanes 5–8*). The faint 55-kDa band in *lane 1* represents background cross-linking to Sec61 due to direct UV irradiation in the absence of the ϵANB probe. There was also a small but variable amount of nonspecific adsorption of translation products to protein A beads (17-kDa band in *lanes 1–3*). A diagram of the construct is indicated below the autoradiogram. The Site of *N*-linked glycosylation (Asn^{42} (*N42*)) is indicated.

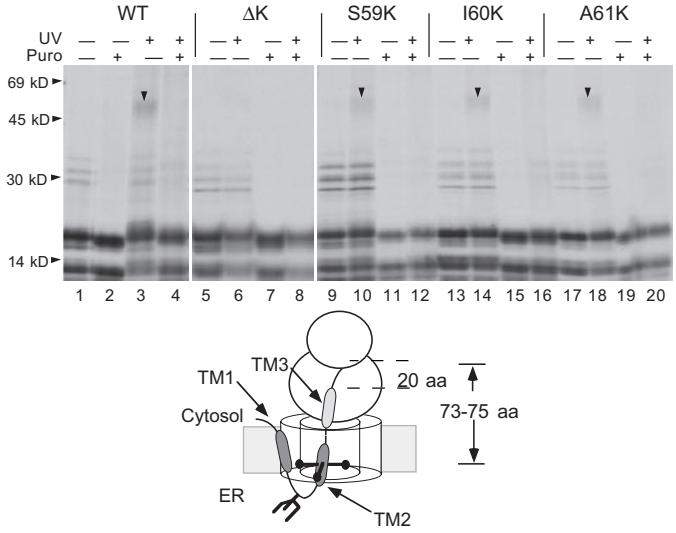

FIGURE 2. **Site-specific TM2-Sec61α cross-linking.** Photocross-linking was performed as described in the legend to Fig. 1 on truncated wild-type AQP1 (*WT*; *lanes 1–4*); a lysine-less AQP1 mutant (*lanes 5–8*); and constructs containing a single Lys residue within TM2 at positions 59–61 (*lanes 9–20*). All samples were translated in the presence of ϵANB-Lys-tRNA and treated with puromycin (*Puro*) and/or UV light as indicated. Photoadducts (*downward arrowheads*) were observed only in chains containing ϵANB-Lys prior to puromycin release (*lanes 3*, *10*, *14*, and *18*). The diagram shows the predicted architecture of the arrested translocation intermediate. The locations of probes (*black circles*) relative to the ribosome PTC and predicted locations of TM2 and TM3 within the ribosome-translocon complex are indicated.

membrane by TM1 before TM2 emerges from the ribosome (31, 32). Constructs were truncated at residue 134, translated in the presence of ϵANB-Lys-tRNA, and cross-linked as described above. At this truncation, probes in TM2 are 73–75 residues from the ribosome PTC, which should position them well outside of the ribosome exit tunnel (9, 10, 41). As shown in Fig. 2, little UV light-dependent cross-linking was observed for the ΔK construct (*lanes 5–8*), but photoadducts were clearly formed at each of the engineered Lys residues within the TM2 segment (*lanes 9–20*). Again, cross-linking was dependent upon both UV activation of the ϵANB moiety and the presence of an intact integration intermediate. The size of photoadducts and immunoprecipitation with Sec61α antisera (see Fig. 4) confirmed that all three residues in TM2 were adjacent to Sec61α at a nascent chain length of 134 aa.

Reconstructing TM2 Movement through Sec61α from Static Translation Intermediates—Because translation of a truncated mRNA generates polypeptides of uniform length, each biosynthetic intermediate provides a static "snapshot" of the molecular environment of the nascent polypeptide at a particular stage of synthesis. We therefore systematically truncated AQP1 mRNA to reconstruct changes in the environment of TM2 as it moved from the ribosome into and through the translocon during nascent chain elongation. Truncated mRNAs containing a unique Lys codon at residue 59, 60, or 61 were generated from PCR-amplified DNA templates as described under "Experimental Procedures." Photocross-linking of arrested integration intermediates revealed a clear pattern in which the position and orientation of TM2 relative to Sec61α were highly dependent on the distance between the probes and the PTC (Fig. 3). Obvious TM2 photoadducts were observed at nascent chain lengths of 97, 105, 110, 118, and 126 in which probes were located 37, 45, 50, 58, and 66 residues from the PTC, respectively (lengths are to the middle probe position). This is in good agreement with the timing of TM2 entry into the translocon for the related aquaporin AQP4 protein (11). Again, minimal cross-linking was observed for ΔK controls (Fig. 4) (data not shown). Glycosylation also increased as the polypeptide was extended to 126 aa, consistent with Asn^{42} movement into the ER lumen. For unclear reasons, I60K was preferentially glycosylated at short truncations (105 and 110 aa), but glycosylation differences between constructs were not observed at longer chain lengths (>118 aa).

We next determined the relative cross-linking efficiency at each probe incorporation site and for each AQP1 truncation. This was accomplished by first quantitating the amount of protein synthesized and recovered in pelleted microsomes for each translation reaction shown in Fig. 3. Equivalent amounts of [^{35}S]Met-labeled protein from each truncation were then concurrently immunoprecipitated with Sec61α antisera. Samples were resolved by SDS-PAGE, and bands were visualized and quantitated by phosphorimaging. The results shown in Fig. 4*A* reveal a distinct pattern of cross-linking and demonstrate that TM2 remained adjacent to Sec61α for a relatively brief period of translation. Specifically, probes within TM2 were positioned adjacent to Sec61 when they were 37–45 aa from the PTC as residues 97–105 were being synthesized. TM2 cross-linking persisted during the synthesis of ~38 additional residues and markedly decreased at truncation 143 when the ϵANB probe

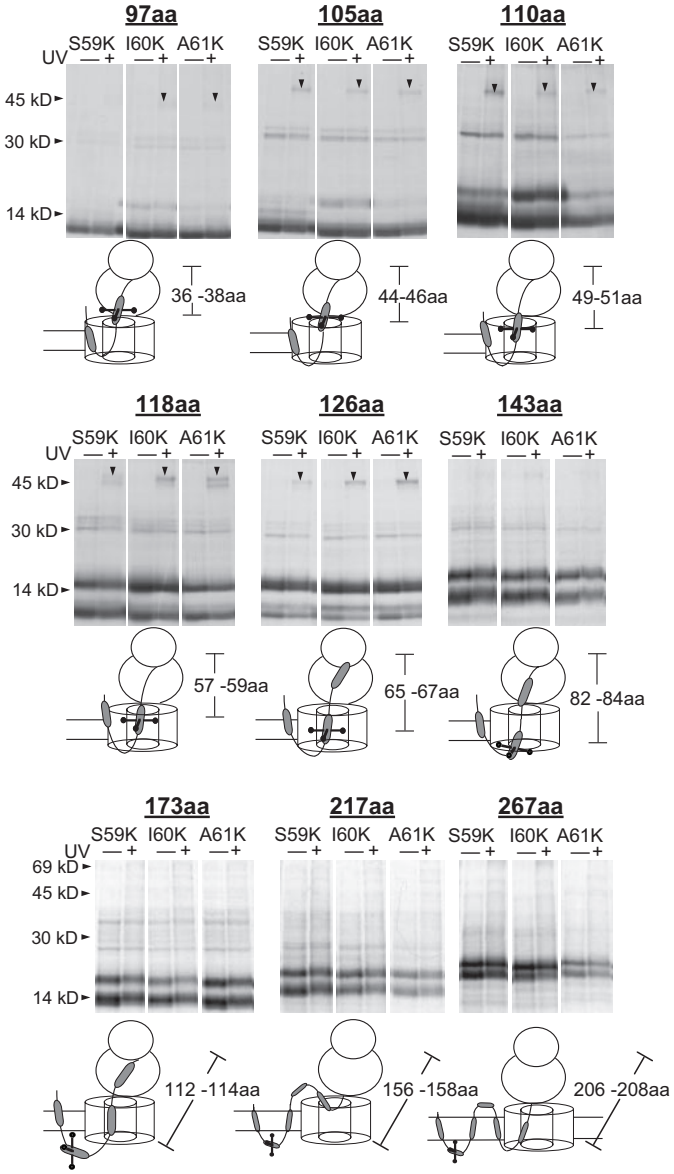

FIGURE 3. **TM2 cross-linking to sequentially arrested integration intermediates.** Truncated AQP1 cDNAs containing a Lys codon at position 59, 60, or 61 were translated in rabbit reticulocyte lysate to generate a series of arrested translocation intermediates. The truncation site for each construct is indicated above the autoradiograms. *Arrowheads* indicate UV light-dependent photoadducts. The diagrams below each autoradiogram represent a model for the predicted location of TM2 at each nascent chain length. The distance of TM2 from the ribosome PTC (in aa) is shown. Note that TM2 is shown exiting the translocon into the ER lumen based on previous studies demonstrating that only TM1, TM3, TM5, and TM6 co-translationally span the ER membrane (31–33, 51).

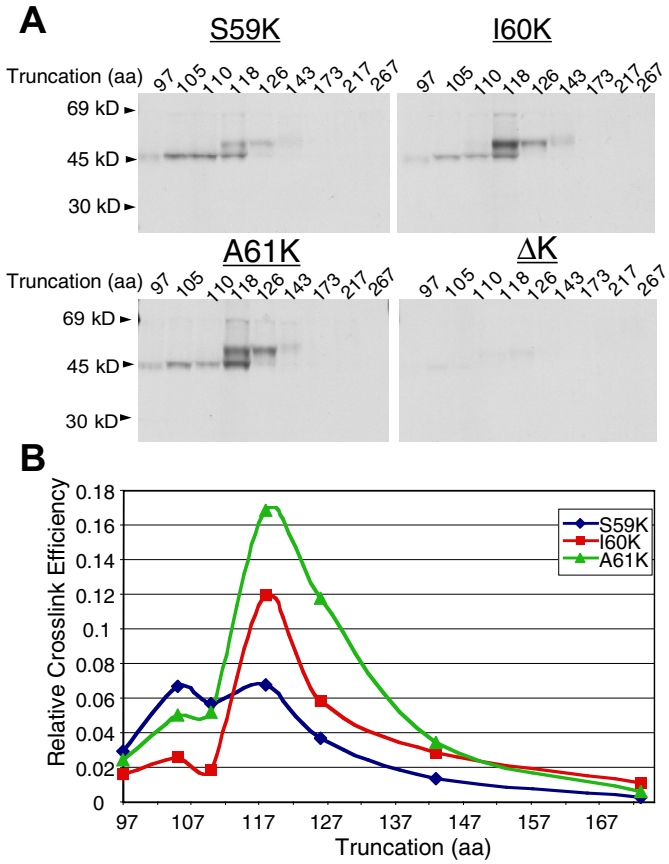

FIGURE 4. **Specific phases of TM2-Sec61α cross-linking.** *A*, AQP1-Sec61α photoadducts were immunoprecipitated and analyzed by SDS-PAGE and autoradiography as described under "Experimental Procedures." The sites of ϵANB probe incorporation and the lengths of integration intermediates are shown above the autoradiograms. The doublet observed at truncation 118 is due to partial *N*-linked glycosylation at Asn[42] (31). Glycosylated photoadducts for shorter truncations, particularly I60K, are visible only upon longer exposure because of the low glycosylation and cross-linking efficiencies. *B*, photoadducts from two independent experiments were quantified by phosphorimaging, and the relative signal intensity at each probe site was plotted as a function of nascent chain length. The data show distinct phases of TM2-translocon interactions and asymmetry of Sec61α cross-linking for nascent chain lengths of 118–143 residues.

was ~86 residues from the PTC. Cross-linking was also observed for both glycosylated and non-glycosylated polypeptides as shown by the doublet present at truncation 118. The relative amount of glycosylated photoadduct generally reflected the glycosylation efficiency as observed upon overexposure of gels (data not shown). As expected, very little Sec61α-reactive material was recovered from ΔK constructs that did not incorporate the ϵANB-Lys probe (ΔK control).

Because equivalent amounts of ^{35}S-labeled protein were immunoprecipitated and all samples were processed and imaged simultaneously, the photoadduct intensity provides a direct comparison of the photocross-linking efficiency and, within the constraints of nitrene group reactivity, the proximity of the ϵANB probe to Sec61α. We therefore plotted the relative cross-linking efficiency *versus* nascent chain length to obtain a profile of TM2-Sec61α interactions at each incorporation site. This approach allowed us to detect subtle differences in the positioning of TM2 within the translocon (Fig. 4*B*) and to identify several distinct phases of TM2-Sec61α photocross-linking. The first phase occurred at nascent chain lengths of 97–105 residues and was characterized by relatively weak cross-linking at all three probe incorporation sites. A second phase of stronger cross-linking was observed, beginning after the synthesis of residue 110 and peaking during the synthesis of residues 118–126. TM2 then left the vicinity of Sec61α after synthesis of residue 143. During the second phase, when TM2 was most proximal to Sec61α, there was significant asymmetry in photocross-linking to different faces of the putative TM helix (residues 61, 60 > 59), indicating that the ϵANB probe did not have equal access to Sec61α even though it was incorporated at adja-

cent residues. These combined results indicate that residues 59–61 initially enter the translocon in an environment that allows relatively limited Sec61α contact and then move into a more proximal location characterized by highly asymmetric cross-linking. This is consistent with entry of the TM into a binding site within the translocon that restricts helix movement (11, 38, 39, 42–46).

TM2 Transiently Withdraws from Sec61α during Translocon Entry—The sharp transitions observed for TM2 cross-linking at specific polypeptide lengths initially suggested that TM2 moves into, through, and out of the translocon as the nascent chain is progressively elongated. However, it was somewhat surprising that synthesis of nearly 20 residues was required between the points at which initial and maximal photocross-linking were observed (residues 97 and 118, respectively). Because 21 fully extended residues would span ~70 Å, a distance significantly greater than the 50 Å thickness of the ER membrane, this suggested that additional factors might affect TM2 progression. We therefore examined the initial phase of TM2 entry in greater detail by introducing unique Lys codons at three additional sites, Phe[56], Gly[57], and Leu[58]. Because these sites were located three residues closer to the N terminus of AQP1, the mRNA was also truncated three codons earlier (residues 94, 102, 107, 115, 123, and 140). In this way, the number of residues between the PTC and ϵANB probe was kept constant, although the latter truncations reflect a slightly earlier stage of translation (by three residues) than those shown in Fig. 4.

Each probe at positions 56–58 generated Sec61α-specific cross-links upon entering the translocon (Fig. 5*A*). Again, the Sec61α cross-linking profiles indicate major transitions in the spatial positioning of TM2 for polypeptides that differed in length by only a few residues. The most striking feature was the increased biphasic nature of TM2 photocross-linking. As the nascent chain increased in length from 94 to 102 residues, a sharp increase in the efficiency of cross-linking to all three probe sites was observed, thereby demonstrating the entry of TM2 into the translocon (Fig. 5*B*). However, synthesis of only five additional residues (truncation 107) resulted in an abrupt and significant decrease in photocross-linking efficiency ($p < 0.05$) (Fig. 5, *B* and *C*). When the nascent chain was lengthened by another 8–16 aa, photocross-linking to residues 56 and 58, but not residue 57, was restored (Fig. 5*C*). This pattern persisted until TM2 was no longer proximal to Sec61α (truncation 158). The overall pattern for residues 56–58 was similar to that observed for residues 59–61 (Fig. 4) with the notable exception that the initial phase of TM2 interactions was more pronounced (discussed below). Biphasic photocross-linking patterns were also observed at additional truncation sites (truncations 97, 105, 110, and 118) and for residues 62–64 (data not shown).

TM2 Entry into the Translocon Is Affected by Nascent Polypeptide Structure in the Ribosome—The photocross-linking profiles obtained for residues 56–58 (Fig. 5*B*) suggested the following scenario. At a nascent chain length of 102 aa, these probes are positioned outside the ribosome exit tunnel and in close proximity to Sec61α. All three probes then move to a site farther away from Sec61α during synthesis of residues 102–107 and return to Sec61 as the nascent chain is lengthened to 123

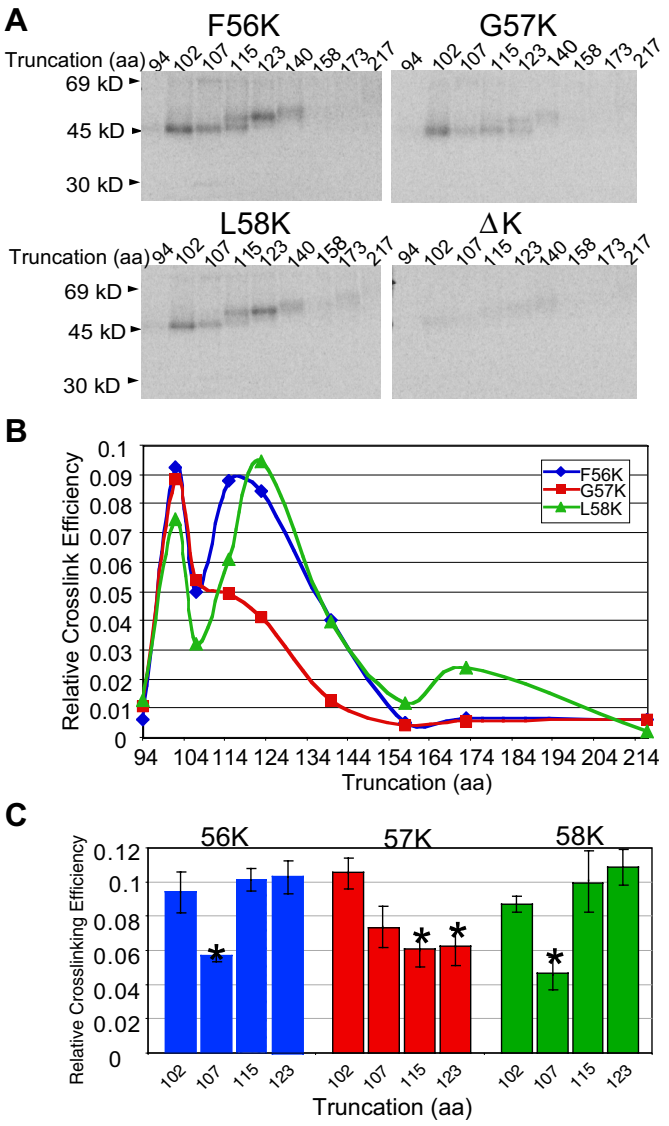

FIGURE 5. **TM2 transient withdrawal from Sec61α during AQP1 synthesis.** Photocross-linking, immunoprecipitation, and quantification were performed as described in the legend to Fig. 4. Probes were positioned in AQP1 at residues 56–58, and truncations were moved three residues toward the N terminus to maintain the number of aa between the probe and PTC as in Fig. 4. *A*, autoradiograms of immunoprecipitated Sec61α photoadducts. *B*, relative photocross-linking efficiencies for each probe site plotted against chain length. *C*, normalized Sec61α photocross-linking efficiencies at truncations 102, 107, 115, and 123 ($n = 4 \pm$ S.E.). *, significant difference from truncation 102 ($p < 0.05$; Student's *t* test).

residues, but in a different molecular environment characterized by enhanced cross-linking to residues 56 and 58 *versus* residue 57. Movement of probes away from Sec61α was tightly coupled to the polypeptide length at truncations 102–115, which also resulted in a minor but reproducible decrease in photocross-linking to residues 59–61 at similar nascent chain lengths (Fig. 4*B*). These data indicate that a substantial portion of TM2 is transiently displaced from Sec61α during a very short interval of protein synthesis. Such a displacement might reflect a lateral repositioning within the translocon that shields TM2 from Sec61α. Alternatively, it seemed plausible that the pattern observed might reflect changes in the location of TM2 along the axial translocation pathway that were dependent upon the

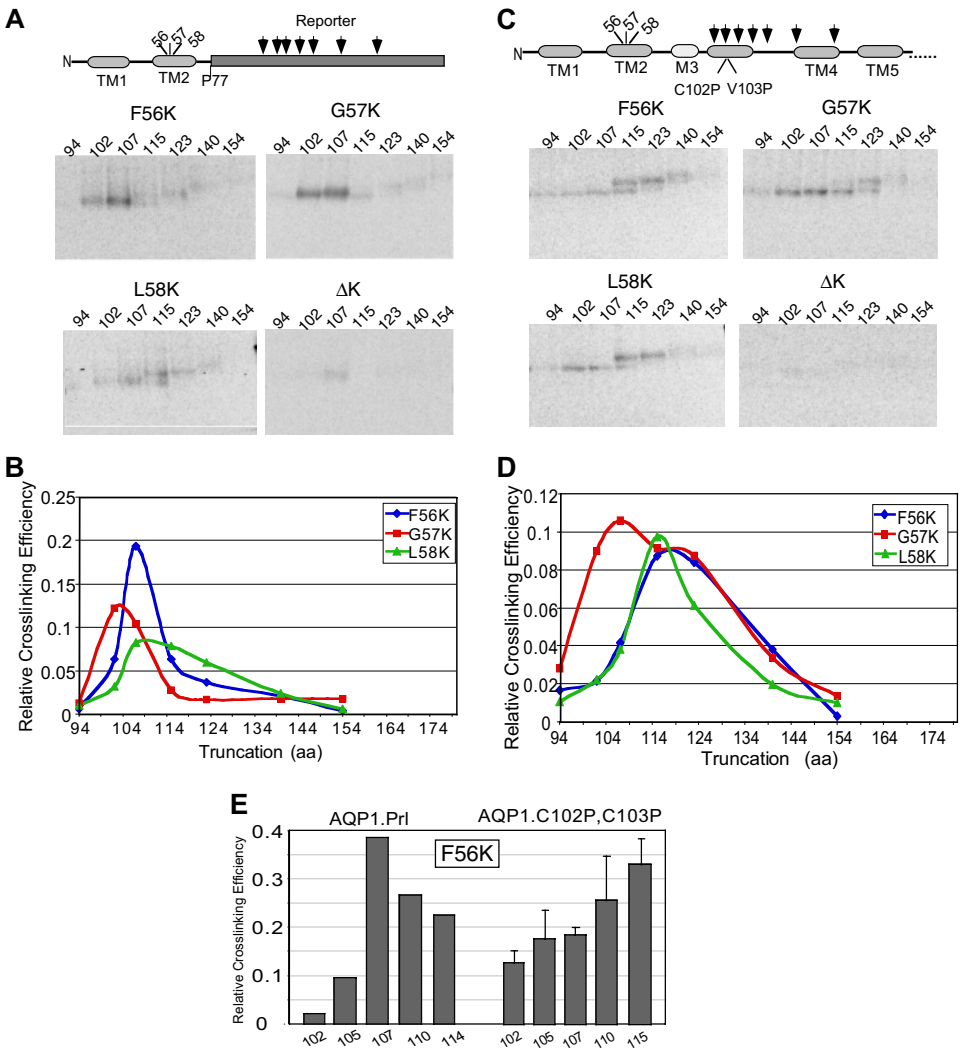

FIGURE 6. **Nascent chain structure within the ribosome influences TM2 entry into Sec61α.** *A*, AQP1 residues C-terminal to Pro[77] were replaced with a secretory passenger domain derived from preprolactin (31), and Sec61α photoadducts to residues 56–58 were analyzed by SDS-PAGE. Truncation sites in the passenger domain (*arrows*) were chosen to maintain the same number of residues between the probes and the PTC as described in the legend to Fig. 5. *B*, photoadduct quantitation revealed that replacing TM2 C-terminal flanking residues within the ribosome exit tunnel markedly shortened the duration of TM2 cross-linking (truncations 102–124) and eliminated transient withdrawal of TM2 at truncation 107. *C* and *D*, experiments were performed as described for *A* and *B* except that truncated AQP1 constructs contained C102P and V103P mutations in TM3. Proline mutations eliminated TM2 withdrawal at truncation 107 but had little effect on the timing of TM2 movement away from Sec61α. *E*, shown is normalized Sec61α photocross-linking to F56K at closely spaced truncations 102, 105, 107, 110, and 114 or 115 in the AQP1-prolactin (*Prl*) fusion protein and proline mutant.

length and structure of the nascent chain in the ribosome exit tunnel. We therefore tested this latter possibility by varying the composition of polypeptide connecting TM2 to the PTC.

The AQP1 coding sequence extending through Pro[77] was fused to a 142-residue secretory passenger domain derived from bovine prolactin (31). These constructs encode the AQP1 N terminus, TM1, TM2, and nine C-terminal residues flanking TM2, but lack TM3 and other downstream residues (Fig. 6*A*). Endogenous Lys codons in the passenger domain were removed such that each construct contained only a single Lys codon for ϵANB-Lys incorporation at position 56, 57, or 58 (or none for ΔK controls). Chimeras were then truncated at lengths identical to those used for cross-linking experiments shown in Fig. 5, and the profiles of Sec61α photocross-linking were determined as described above. As shown in Fig. 6 (*A* and *B*), removal of TM3 and other downstream residues caused a marked change in the TM2 photocross-linking profile (compare with Fig. 5*B*). Most notably, Sec61α photocross-linking peaked at truncation 107 and decreased markedly for nascent chains 123 residues and longer. Because N-terminal sequences through residue 77 and the number of residues between the probe and the PTC were identical for the experiments shown in Figs. 5 and 6, any differences must be due to composition of the nascent chain located within the ribosome exit tunnel. Thus, replacing a natural AQP1 sequence downstream of TM2 with a secretory protein sequence appears to accelerate TM2 progression through the translocon.

Proline Insertion into TM3 Eliminates TM2 Withdrawal from Sec61α—When TM2 is temporarily displaced from Sec61α (truncation 107) (Fig. 5*B*), the C-terminal end of TM2 is separated from the PTC by 39 residues. The AQP1 crystal structure indicates that this peptide region contains a short helix designated M3 (Asn[76]–Cys[87]) as well as the first 14 residues of TM3 (30). This raised the intriguing possibility that the compaction of a helical region, either TM3 or the M3 segment, might influence the movement of TM2 along the translocation pathway, thereby causing TM2 to temporarily withdraw toward the ribosome exit tunnel. Such a conformational change might occur if a portion of extended nascent polypeptide (~3.5 Å/aa) were converted into an α-helical conformation (1.5 Å/aa). Depending on the number of residues involved and the kinetics of helix formation, the resulting compaction of the nascent chain could significantly alter the proximity of the photoreactive probes relative to Sec61α.

To test whether TM3 secondary structure influences TM2 movement through Sec61α, two proline residues (C102P and V103P) were introduced into the AQP1 construct (Fig. 6*C*). This creates a tripeptide Pro-Pro-Gly sequence near the middle of TM3 that would be predicted to disrupt helix formation. Lys residues were then introduced into this AQP1 proline mutant background at positions 56–58, and photocross-linking to Sec61α was examined in polypeptides truncated at residues 94, 102, 107, 115, 123, 140, and 154. The results in Fig. 6 (*C* and *D*) show that the proline mutations eliminated transient with-

drawal of TM2 from Sec61α at truncation 107. AQP1-PP nascent chains also exhibited a broad peak of TM2 cross-linking in which the timing of TM2 exit from the translocon was similar to that observed for AQP1 constructs containing a native TM3 sequence (truncations 140–154). To ensure that cross-linking did not transiently decrease between truncations 102 and 115, the F56K construct was re-examined at closely spaced truncations in this region for both the AQP1 fusion protein and the proline mutants (Fig. 6*E*). In each case, the cross-linking efficiency continued to increase during synthesis, indicating that all three probes moved continuously toward a site proximal to Sec61α. Notably, AQP1-PP differs from the wild-type protein sequence only by the presence of two proline residues within TM3. Thus, the sequence and/or structure of the nascent protein within the exit tunnel has a profound impact on how TMs exiting the ribosome are presented to the ER translocation machinery.

DISCUSSION

In this study, we have used a modified aminoacyl-tRNA to incorporate photoactive probes into a nascent polytopic membrane protein TM and to monitor its movement into and through the Sec61 translocon during co-translational integration at the ER membrane. A key aspect of this study was the ability to quantitatively compare photocross-linking efficiencies at multiple positions within a single TM. Whereas photocross-linking to any one residue might reflect local fluctuations in accessibility, reactivity, and/or quenching of the nitrene group, multiple probe insertion sites on different faces of the putative helix over a significant length of TM2 provide a relatively cohesive picture of TM2 proximity to Sec61α. Furthermore, systematic lengthening of the nascent chain allowed us to identify subtle changes in molecular environment and to reconstruct transitions experienced by the TM during its passage through the translocation pathway.

Several striking features of the data were apparent. First, major transitions in Sec61α photocross-linking efficiency were observed over remarkably small incremental changes in nascent chain length. Thus, the environment of a TM within the translocon is closely coordinated with and dependent upon polypeptide elongation at the ribosome PTC. Second, the coordinated timing of the transitions observed for different probe sites identified distinct phases of TM2-translocon interactions. The first phase occurred at a nascent chain length of 94–107 aa and was characterized by a brief period of Sec61α photocross-linking to TM2 residues 56–61. Although not compared directly, photocross-linking during this phase appeared to be more efficient for probe locations closer to the TM2 N terminus (residues 56–58) than to the more C-terminal residues 59–61. Thus, at this point of synthesis, TM2 likely emerges from the ribosome exit tunnel and contacts the translocon in an N- to C-terminal direction. The second phase occurred at a chain length of 107–110 aa and was characterized by an abrupt decrease in cross-linking efficiency, most notably for residues 56–58. TM2 therefore appears to move to a location more distant from Sec61α than it had occupied in the first phase. The third phase (synthesis of residues 115–126) was characterized by a period of photocross-linking in which TM2 resided in close proximity to Sec61α. Although the photocross-linking pattern during this phase did not reveal a clear helical periodicity, the strong asymmetry indicates that TM2 movement was restricted and that its positioning adjacent to translocon proteins was nonrandom. This is consistent with TM2 entering a specific binding site that is formed by and/or adjacent to Sec61α, as has been suggested previously (11, 38, 39, 46, 47). The fourth and final phase was marked by the loss of Sec61α photocross-linking and the release of TM2 from the translocon at a chain length of >143 residues.

The most surprising discovery was the non-continuous passage of TM2 into and through the translocon as the nascent chain increased in length from 94 to 118 residues. Photocross-linking patterns obtained for multiple probe locations and truncation sites are most consistent with initial entry of the N terminus of TM2 into Sec61α during the first phase, followed by a temporary withdrawal from the translocon during the second phase and then a subsequent re-entry into the translocon during the third phase. This contrasts with models predicting that nascent chain elongation results in progressive movement through the aqueous ribosome exit tunnel and the aligned Sec61 protein-conducting pore (48–50).

Several lines of evidence indicate that the increased separation between AQP1 TM2 and Sec61α during the second phase is more likely to result from TM2 movement within the axial translocation pathway than from a rearrangement of the membrane-bound ribosome-translocon complex or transient lateral partitioning into the lipid bilayer. First, the decrease in Sec61α cross-linking to residues 56–58 was both abrupt and transient, occurring during synthesis of only a few amino acids. Second, the decrease in Sec61α photocross-linking was not accompanied by a noticeable increase in cross-linking to other translocon components (TRAM or TRAP) (data not shown). Third, AQP1 TM2 is too hydrophilic to terminate translocation and co-translationally span the membrane (31–33, 51), thereby making a transient lateral partitioning into the lipid bilayer highly unlikely.

How then is the relocation of TM2 within the axial translocation pathway accomplished? Whereas several studies have suggested that nascent polypeptides maintain an extended conformation as they traverse the ribosome-translocon complex (41, 52, 53), certain nascent chains have been shown to acquire a compact conformation (54–57). In one recent study, fluorescence resonance energy transfer between donor and acceptor dyes positioned 24 residues apart in a secretory protein revealed a low fluorescence resonance energy transfer efficiency, whereas the same dyes positioned at opposite ends of a TM (also 24 residues apart) exhibited a large increase in fluorescence resonance energy transfer shortly after the TM left the PTC (27). These results indicate that the secretory protein segment was largely extended inside the ribosome, whereas dyes spanning the TM had moved much closer together (27). Cysteine accessibility studies using alkylating agents support these findings and show that peptide regions with high helical propensity can also significantly shorten the effective nascent polypeptide length within the ribosome exit tunnel (58, 59).

The above results therefore suggest a plausible explanation for our observations, *viz.* that TM2 is transiently drawn back either into the ribosome exit tunnel or toward the ribosome-translocon interface at a chain length of 107–110 aa. If a portion of the nascent chain folds into a more compact structure inside the ribosome, and one end of the nascent chain is fixed at the PTC, then the other end of the nascent chain must move to allow the observed contraction. Regions of TM2 near the exit site would therefore be expected to move back toward the tunnel. Because the most likely AQP1 sequence to undergo folding inside the ribosome is TM3, we examined whether its presence or absence affects the temporary withdrawal of TM2 from Sec61α. When residues following TM2 were replaced with a secretory passenger protein, no decrease in cross-linking was observed during the second phase. These results demonstrate that withdrawal of TM2 from the translocon is not due to specific properties of TM2, but is instead dependent upon TM2 C-terminal flanking residues. In addition, introduction of two helix-destabilizing residues within the TM3 segment eliminated the transient decrease in photocross-linking observed at residue 107. Because all AQP1 residues, including TM2, were otherwise identical at each truncation, the cause of TM2 withdrawal must be attributed to the change in the primary and/or secondary structure of TM3.

Our results thus support a model in which TM3 folding elicits a shortening of the nascent polypeptide within the ribosome exit tunnel. If TM3 adopted a more compact and perhaps helical conformation after the addition of residue 107 (when 14 TM3 residues have been synthesized), then the shortening of its end-to-end distance from ~50 Å (extended) to ~20 Å (helical) would be sufficient to withdraw TM2 residues away from Sec61α if they were initially positioned close to the ribosome-translocon interface. Of course, this situation would be temporary because residues 56–58 would again reach Sec61α as translation continues, thus giving rise to the biphasic pattern of cross-linking observed. Although the entire AQP1 folding pathway is not yet fully understood, AQP1 biogenesis in the rabbit reticulocyte lysate system has been shown to faithfully reconstitute co-translational integration observed in intact cells (33, 51). Our results therefore likely reflect events that occur during native polytopic protein biogenesis and reveal that nascent chain movement during co-translational integration is complex and subject to control by TM-dependent nascent chain folding. Given the spectrum of folding possibilities shown both experimentally (27, 58–60) and theoretically (61, 62), it will be intriguing to discover the functional and regulatory ramifications of altering nascent chain interactions with the translocon in response to co-translational polypeptide folding.

Acknowledgments—We thank Dr. Kent Matlack for the generous gift of Sec61 antisera; Dr. Isaiah Turnbull for technical expertise; and Drs. Heather Sadlish, Peter McCormick and members of the Skach laboratory for helpful comments.

REFERENCES

1. Johnson, A., and van Waes, M. (1999) *Annu. Rev. Cell Dev. Biol.* **15,** 799–842
2. Schnell, D., and Hebert, D. (2003) *Cell* **112,** 491–505
3. Song, W., Raden, D., Mandon, E., and Gilmore, R. (2000) *Cell* **100,** 333–343
4. Crowley, K., Reinhart, G., and Johnson, A. (1993) *Cell* **73,** 1101–1115
5. Crowley, K., Liao, S., Worrell, V., Reinhart, G., and Johnson, A. (1994) *Cell* **78,** 461–471
6. Beckmann, R., Bubeck, D., Grassuicci, R., Panczek, P., Verschoor, A., Blobel, G., and Frank, J. (1997) *Science* **278,** 2123–2126
7. Rapoport, T., Goder, V., Heinrich, S., and Matlack, K. (2004) *Trends Cell Biol.* **14,** 568–575
8. Krieg, U., Johnson, A., and Walter, P. (1989) *J. Cell Biol.* **109,** 2033–2043
9. Mothes, W., Prehn, S., and Rapoport, T. (1994) *EMBO J.* **13,** 3973–3982
10. Ban, N., Nissen, P., Hansen, J., Moore, P., and Steitz, T. (2000) *Science* **289,** 905–920
11. Sadlish, H., Pitonzo, D., Johnson, A., and Skach, W. R. (2005) *Nat. Struct. Mol. Biol.* **12,** 870–878
12. Perara, E., Rothman, R. E., and Lingappa, V. R. (1986) *Science* **232,** 348–352
13. Hoffman, K. E., and Gilmore, R. (1988) *J. Biol. Chem.* **263,** 4381–4385
14. Lu, Y., Xiong, X., Helm, A., Kimani, K., Bragin, A., and Skach, W. R. (1998) *J. Biol. Chem.* **273,** 568–576
15. Denzer, A., Nabholz, C., and Spiess, M. (1995) *EMBO J.* **14,** 6311–6317
16. Goder, V., Bieri, C., and Spiess, M. (1999) *J. Cell Biol.* **147,** 257–266
17. Ooi, C., and Weiss, J. (1992) *Cell* **71,** 87–96
18. Simon, S., Peskin, C., and Oster, G. (1992) *Proc. Natl. Acad. Sci. U. S. A.* **89,** 3770–3774
19. Helenius, A., Marquardt, T., and Braakman, I. (1992) *Trends Biochem. Sci.* **2,** 227–231
20. Matlack, K., Misselwitz, B., Plath, K., and Rapoport, T. (1999) *Cell* **97,** 553–564
21. Hamman, B., Hendershot, L., and Johnson, A. (1998) *Cell* **92,** 747–758
22. Jungnickel, B., and Rapoport, T. (1995) *Cell* **82,** 261–270
23. Belin, D., Bost, S., Vassalli, J.-D., and Strub, K. (1996) *EMBO J.* **15,** 468–478
24. Liao, S., Lin, J., Do, H., and Johnson, A. (1997) *Cell* **90,** 31–42
25. Haigh, N., and Johnson, A. (2002) *J. Cell Biol.* **156,** 261–270
26. Alder, N., Shen, Y., Brodsky, J., Hendershot, L., and Johnson, A. (2005) *J. Cell Biol.* **168,** 389–399
27. Woolhead, C., McCormick, P., and Johnson, A. (2004) *Cell* **116,** 725–736
28. Agre, P., King, L., Yasui, M., Guggino, W., Ottersen, O., Fujiyoshi, Y., Engel, A., and Nielsen, S. (2002) *J. Physiol.* (*Lond.*) **542,** 3–16
29. Fu, D., Libson, A., Miercke, L., Weitzman, C., Nollert, P., Krucinski, J., and Stroud, R. (2000) *Science* **290,** 481–486
30. Sui, H., Han, B.-G., Lee, J., Walian, P., and Jap, B. (2001) *Nature* **414,** 872–878
31. Skach, W. R., Shi, L.-B., Calayag, M. C., Frigeri, A., Lingappa, V. R., and Verkman, A. S. (1994) *J. Cell Biol.* **125,** 803–815
32. Foster, W., Helm, A., Turnbull, I., Gulati, H., Yang, B., Verkman, A. S., and Skach, W. R. (2000) *J. Biol. Chem.* **275,** 34157–34165
33. Lu, Y., Turnbull, I. R., Bragin, A., Carveth, K., Verkman, A. S., and Skach, W. R. (2000) *Mol. Biol. Cell* **11,** 2973–2985
34. Buck, T., Wagner, J., Grund, S., and Skach, W. R. (2007) *Nat. Struct. Mol. Biol.* **14,** 762–769
35. Ho, N., Hunt, H., Horton, R., Pullen, J., and Pease, P. (1989) *Gene* (*Amst.*) **77,** 51–59
36. Oberdorf, J., and Skach, W. R. (2002) in *Methods in Molecular Medicine–Cystic Fibrosis: Methods and Protocols* (Skach, W. R., ed) p. 70, Humana Press Inc., Totowa, NJ
37. Krieg, U., Walter, P., and Johnson, A. (1986) *Proc. Natl. Acad. Sci. U. S. A.* **83,** 8604–8608
38. McCormick, P., Miao, Y., Shao, Y., Lin, J., and Johnson, A. (2003) *Mol. Cell* **12,** 329–341
39. Saksena, S., Shao, Y., Braunagel, S., Summers, M., and Johnson, A. (2004) *Proc. Natl. Acad. Sci. U. S. A.* **101,** 12537–12542
40. Heinrich, S., and Rapoport, T. (2003) *EMBO J.* **22,** 3654–3663
41. Matlack, K. E. S., and Walter, P. (1995) *J. Biol. Chem.* **270,** 6170–6180
42. Do, H., Falcone, D., Lin, J., Andrews, D., and Johnson, A. (1996) *Cell* **85,** 369–378
43. Meacham, G., Patterson, C., Zhang, W., Younger, J., and Cyr, D. (2001)

Nat. Cell Biol. **3,** 100–105
44. Ismail, N., Crawshaw, S., and High, S. (2006) *J. Cell Sci.* **119,** 2826–2836
45. Cannon, K. S., Or, E., Clemons, W., Shibata, Y., and Rapoport, T. (2005) *J. Cell Biol.* **169,** 219–225
46. Plath, K., Wilkinson, B., Stirling, C., and Rapoport, T. (2004) *Mol. Biol. Cell* **15,** 1–10
47. Pitonzo, D., and Skach, W. R. (2006) *Biochim. Biophys. Acta* **1758,** 976–988
48. Morgan, D., Menetret, J.-F., Neuhof, A., Rapoport, T., and Akey, C. (2002) *J. Mol. Biol.* **324,** 871–886
49. Beckmann, R., Spahn, C., Eswar, N., Helmers, J., Penczek, P., Sali, A., Frank, J., and Blobel, G. (2001) *Cell* **107,** 361–372
50. Menetret, J.-F., Hegde, R., Heinrich, S., Chandramouli, P., Ludtke, S., Rapoport, T., and Akey, C. (2005) *J. Mol. Biol.* **348,** 445–457
51. Buck, T. M., and Skach, W. R. (2005) *J. Biol. Chem.* **280,** 261–269
52. Kowarik, M., Kung, S., Martoglio, B., and Helenius, A. (2003) *Mol. Cell* **10,** 735–744
53. Whitley, P., Nilsson, I., and von Heijne, G. (1996) *J. Biol. Chem.* **271,** 6241–6244
54. Picking, W., Picking, W., Odom, O., and Hardesty, B. (1992) *Biochemistry* **331,** 2368–2375
55. Tsalkova, T., Odom, O., Kramer, G., and Hardesty, B. (1998) *J. Mol. Biol.* **278,** 713–723
56. Mingarro, I., Nilsson, I., Whitley, P., and von Heijne, G. (2000) *BMC Cell Biol.* **1,** 3
57. Kramer, G., Ramachandrian, V., and Hardesty, B. (2001) *Int. J. Biochem. Cell Biol.* **33,** 541–553
58. Lu, J., and Deutsch, C. (2005) *Biochemistry* **44,** 8230–8243
59. Lu, J., and Deutsch, C. (2005) *Nat. Struct. Mol. Biol.* **12,** 1123–1129
60. Woolhead, C., Johnson, A., and Bernstein, H. (2006) *Mol. Cell* **22,** 587–598
61. Voss, N., Gerstein, M., Steitz, T., and Moore, P. (2006) *J. Mol. Biol.* **360,** 893–906
62. Ziv, G., Haran, G., and Thirumalai, D. (2005) *Proc. Natl. Acad. Sci. U. S. A.* **102,** 18956–18961